Application of Bayesian Neural Network in Electrical Impedance Tomography

Jouko Lampinen and Aki Vehtari

{Jouko.Lampinen,Aki.Vehtari}@hut.fi

Laboratory of Computational Engineering

Helsinki University of Technology

P.O.Box 9400, FIN-02015 HUT, FINLAND

Kimmo Leinonen

leinonen_kimmo@ccmail.ahlstrom.com

Ahlstrom Pumps Corporation

P.O.Box 18, FIN-48601, Karhula, FINLAND

Abstract

In this contribution we present a method for solving the inverse problem in electric impedance tomography with neural networks. The problem of reconstructing the conductivity distribution inside an object from potential measurements on the surface is known to be ill-posed, requiring efficient regularization techniques. We demonstrate that a statistical inverse solution, where the mean of the inverse mapping is approximated with a neural network gives promising results. We study the effect of input and output data representation by simulations and conclude that projection to principal axis is feasible data transformation. Also we demonstrate that Bayesian neural networks, which aim to average over all network models weighted by the model's posterior probability provide the best reconstruction results. With the presented approach estimation of some target variables, such as the void fraction (the ratio of gas and liquid), may be applicable directly without the actual image reconstruction. We also demonstrate that the solutions are very robust against noise in inputs.

1   Introduction

In electrical impedance tomography (EIT) the aim is to recover the internal structure of an object from surface measurements. Number of electrodes are attached to the surface of the object and current patterns are injected from through the electrodes and the resulting potentials are measured. The inverse problem in EIT, estimating the conductivity distribution from the surface potentials, is known to be severely ill-posed, so that some regularization methods must be used to obtain feasible results [8].

Typically, the inverse problem in EIT is solved by assuming the system linear and computing regularized inverse matrix. This produces fast linear reconstruction algorithm. However the linear assumption is valid only if the perturbation from the linearization point is small, i.e., there are no large areas where conductance differs much from the background.

Another, more accurate approach for the image reconstruction in EIT is based on iterative inversion of the forward problem. Numerical minimization method, such as Newton-Raphson algorithm, is used to search for a conductance distribution that minimizes the difference between the measured potentials and those obtained by computing the potentials by, e.g., finite element method. This approach leads to computationally more complex algorithms, but gives much better results and offers more flexibility for controlling the regularization of the inverse, by defining the smoothing priors for the resulting image [8].

In this study we consider a simulated EIT problem of detecting gas bubbles in circular water pipe. The bubble formations consist of one to ten random overlapping circular bubbles, drawn so that the void fraction (area of the bubbles / area of the pipe) is roughly Gamma distributed with mean of 20%. In the following tests we used 500 samples in the training set and 500 in the test set. Fig. 1 shows an sample bubble and resulting equipotential curves. The potential signals from which the image is to be recovered are shown in Fig. 2.

We present a statistical inverse approach for the EIT problem, based on approximating the inverse mapping with a Multi Layer Perceptron (MLP) neural network. Often the end goal of using process tomography is not the reconstructed image, but some index computed from the image, such as void fraction or mixing index indicating how well two substances have been mixed. We demonstrate that in such situation it may be feasible to directly estimate the target variable without the actual image reconstruction.

There are a few studies on using neural networks in the EIT problem. In [7] the reconstruction image was directly estimated by a neural network from the potential signals.The solution was demonstrated to be very robust against noise in input signals. However, the resolution of the image in such approach is in practice limited to some tens or hundreds of pixels, as networks with several hundreds of outputs are rather difficult to use and train, and often require
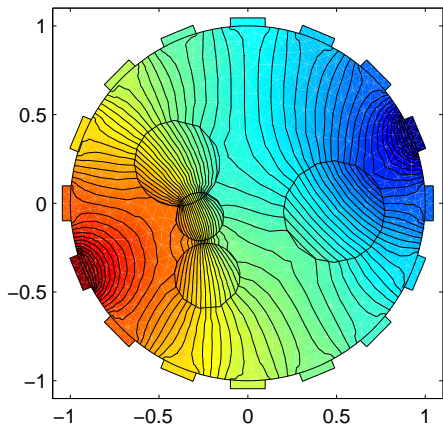
Figure 1: Example of the EIT problem. The simulated bubble is bounded by the circles. The current is injected from the electrode with the lightest color and the opposite electrode is grounded. The color and the contour curves show the resulting potential field.
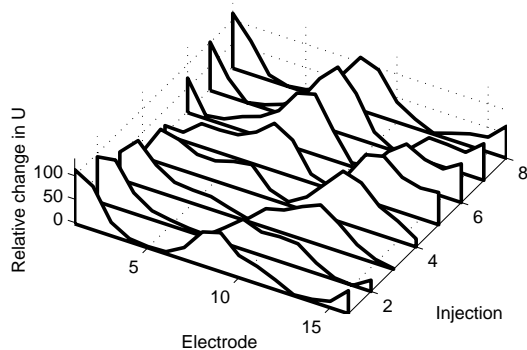

Figure 2: Relative changes in potentials compared to homogeneous background. The eight curves correspond to injections from eight different electrodes.

non-standard regularization to smooth the results of neighboring pixels.

In [1] linear neural network was used to estimate the conductance in the triangles of the FEM mesh. As the used network was linear, the actual advantage over linear pseudoinverse solutions was due to the iterative estimation of the inverse matrix with a gradient method, which proceeds slowly to the direction of the smallest eigenvectors of the inverse matrix, yielding natural regularization for the inverse.

In [6] combination of principal component analysis (PCA) and neural network was used for computing a scalar variable, mixing index, from reconstructed tomographic images.

Our results indicate that direct estimation of the target variables without the explicit reconstruction may be appropriate solution, as the reconstruction may be much more complex problem than the actual end goal.

2 Bayesian Neural Networks

Traditionally neural networks have been trained by searching for a set of weights that minimize the error between the target values and network outputs.

In Bayesian learning the objective is to find the predictive distribution for output y given the input x and training data D (see [2] and [4] for introduction to Bayesian neural networks)

$$p(y|x, D) = \int p(y|x, w, \beta) \frac{p(D|w)p(w|\alpha)p(\alpha)}{p(D)} \, dw\alpha\beta,$$

where we compute the marginal distribution over all the parameters w and hyperparameters α, that determine the prior distributions for parameters, and β, that define the noise variance. Intuitively, the marginalization is equal to taking the average prediction of all the models $p(y|x, w, \beta)$ weighted by their goodness, which is the posterior probability of the model given the training data D.

In practice we use Markov Chain Monte Carlo techniques for approximating the integral by mean of samples drawn from the posterior distribution of the models [4]. In the following experiments we have used the FBM software package [1] that implements the methods described in [4]. The resulting model after the learning is a collection of networks with different parameters w, such that the average of the outputs of the networks approximates the conditional expectation of the output given the input. In this work we have used 20 samples from the posterior distributions, so that the network model is equal to having a committee of 20 networks.

3 Data Representation

One of the key issues in the approach presented here is transformation of both input and output data by principal component projection and application of the neural network in this lower dimensional eigenspace. This serves for three purposes: first to detach the actual inverse problem from the data representation of the potential signals and image data, allowing change of image resolution afterwards by changing the resolution of the eigen images. Secondly, the reconstruction of the image as superposition of the eigen images

---

[1]<URL:http://www.cs.toronto.edu/~radford/fbm.software.html>

makes the inverse more robust against noise, as shown by the experiments. Thirdly, the dimensionality of the reconstruction problem is much reduced, and it is matched to the actual complexity of the bubble distributions (determined by the eigenvalues of the correlation matrix).

The reconstruction equations are then

$$u_p = V_u u$$
$$g_p = F(p) \qquad (1)$$
$$g = V_g^T g_p$$

where

u is the potential signal,

V_u is the base span by the largest eigenvectors of u (we used $N_u = 20$),

u_p is the projection of u on V_u,

g is the reconstructed image,

V_g is the base of eigenvectors of the autocorrelation matrix of the images,

g_p is the projection of the image g on base V_g, and

$F(p)$ is the non-linear function giving the inverse (the Bayesian MLP).

Eigenimages could be computed from the training data [3], but a more principled approach is to construct a model for the autocorrelation of the conductivity distribution and compute the eigen vectors of the autocorrelation matrix. The autocorrelation model we used consisted of position dependent variance term $S(x, y)$ and position independent autocorrelation term $A(\Delta x, \Delta y)$:

$$R_{xy,x'y'} = A(x - x', y - y')S(x, y)S(x', y'), \qquad (2)$$

where we used rather generic assumptions: autocorrelation of pixels decays linearly as function of distance $\sqrt{\Delta x^2 + \Delta y^2}$ and reaches zero correlation at distance 0.5 (half of the radius of the pipe). The variance was modeled as sum of two Gaussians

$$S(x, y) = \sum_{k=1}^{2} Z_k \exp\left(-\frac{x^2 + y^2}{2\sigma_k^2}\right). \qquad (3)$$

where the parameters σ_k and Z_k were determined by maximum likelihood fit to the training data. The resulting base is shown in Fig. 3. Note that we can control the accuracy of image representation in different locations of the image by changing the autocorrelation length. Shorter autocorrelation results in more eigenimages coding the location and vice versa. Eigenimages computed from the autocorrelation model and those from the training data have been compared in [3].

Tables 1 and 2 and Fig. 4 show the effect of using the PCA projection as input or output transformation. The figures are
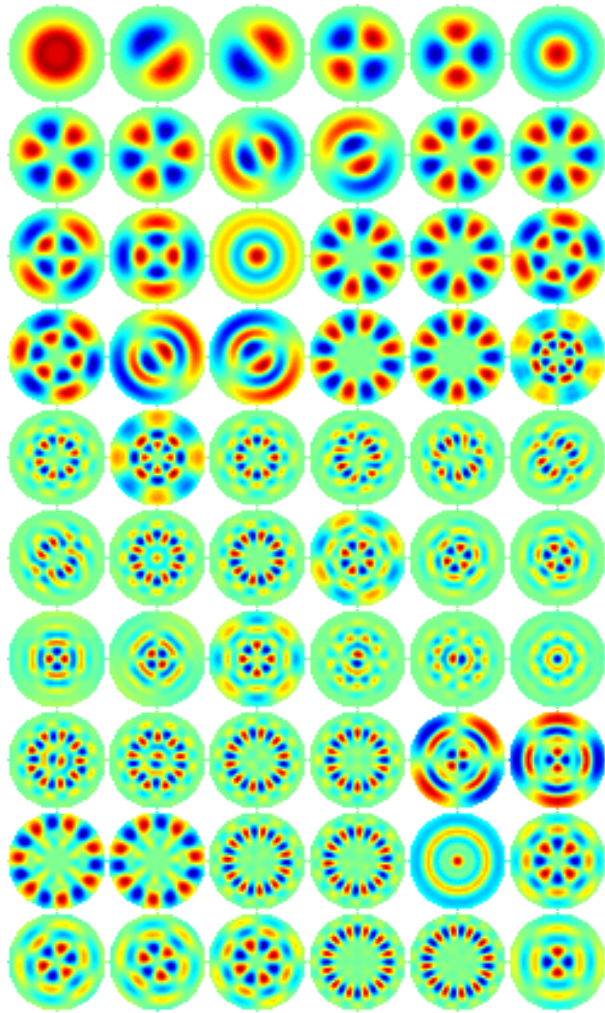

Figure 3: Eigenimages from the autocorrelation model in (2) and (3).

computed with a MLP early stopping committee using different data partition for each member, as it is faster method than the Bayesian MLP. Clearly the best performance is obtained with PCA projection in both ends. Some examples of the reconstructed images are shown in Fig. 5.

4 Reconstruction results

In this section we present results of Bayesian MLP method for the EIT problem. We used one hidden layer MLP with 20 hidden units, per-case normal noise variance model, vague priors and MCMC-run specifications similar as used in [4, 5]. We run five long chains and discarded first half of the each chain. Finally 20 networks from the posterior distribution of network parameters were used. PCA transformation was used for both potential signals and images.
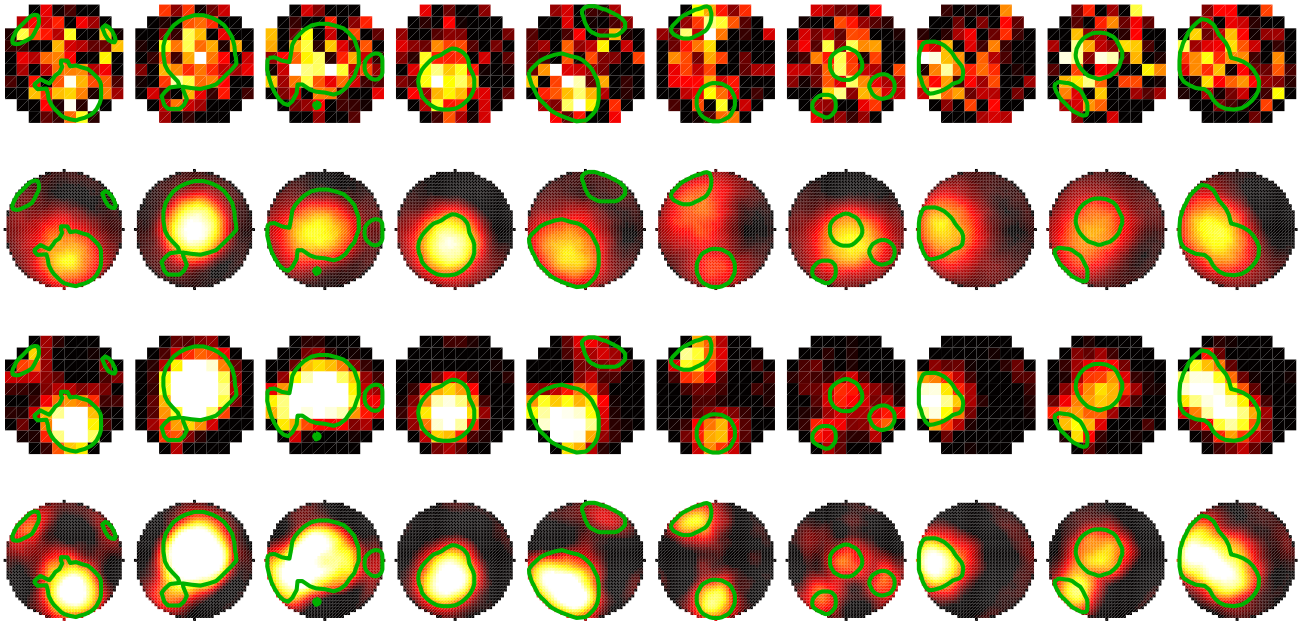
Figure 5: Examples of the effect of data representation. The coding schemes are from up: direct in - direct out, direct in - PCA out, PCA in - direct out, PCA in - PCA out. The color in the figures show the probability of the bubble in each pixel. The data dimensions were: direct in: 256, PCA in: 20, direct out: 88, PCA out: 60.

Table 1: Effect of data coding. Mean relative absolute error in void fraction, $mean(|\hat{v}_f - v_f|/v_f)$, %.

Image coding	Voltage signal coding	
	Direct 256	PCA 20
Direct 10x10	40.3	9.4
PCA 60 (41x41)	46.7	8.7

Table 2: Effect of data coding. Reconstruction error, percentage of erroneously segmented pixels.

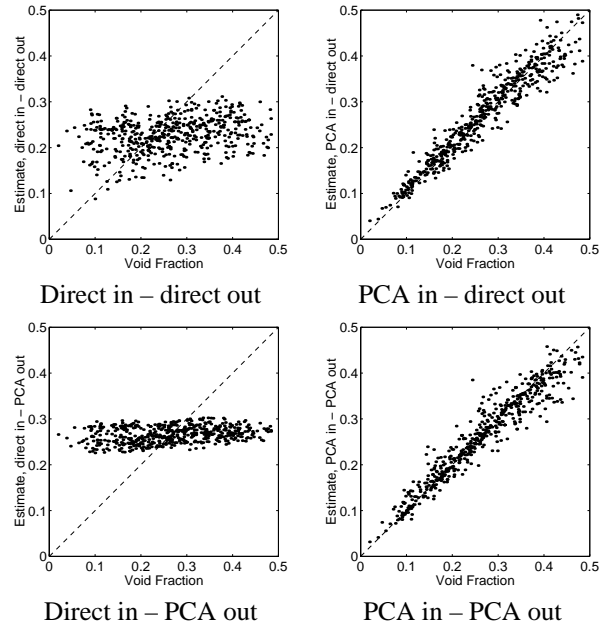| Image coding	Voltage signal coding	
	Direct 256	PCA 20
Direct 10x10	17.5	9.7
PCA 60 (41x41)	14.1	6.7

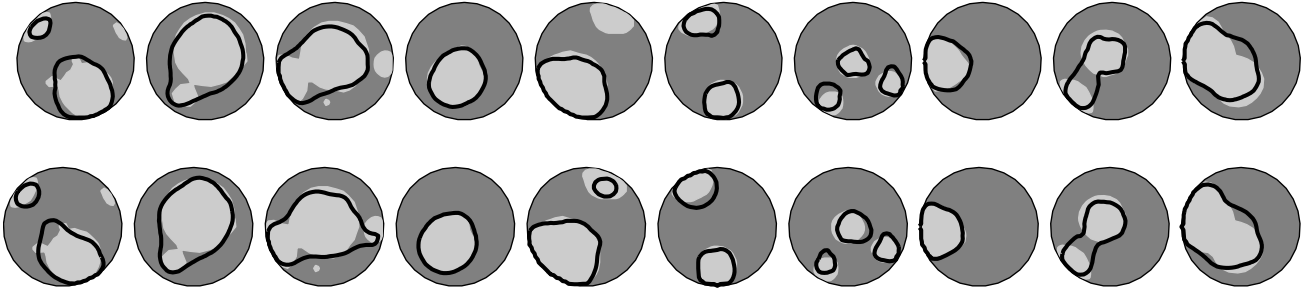Figure 4: Scatter plots of the Void Fraction estimates with different data codings.

Figure 6: Example of image reconstructions with MLP ESC (upper row) and the Bayesian MLP (lower row)

Table 3: Errors in reconstructing the bubble shape and estimating the void fraction from the reconstructed images. See text for explanation of the different models.

Method	Classification errors %	Relative error in void fraction %
MLP ESC	6.7	8.7
Bayesian MLP	5.9	8.1
Bayesian MLP, direct VF		3.4

As baseline result for MLPs we used early stopping committee of 20 MLP networks (MLP ESC), with different division of data to training and stopping sets for each member. The networks were initialized to near zero weights to guarantee that the mapping is smooth in the beginning. When used with caution MLP early stopping committee is good baseline method for neural networks.

Fig. 6 shows examples of the image reconstruction results. Table 3 shows the quality of the image reconstructions with models, measured by error in the void fraction and percentage of erroneous pixels in the segmentation, over the test set.

An important goal in the studied process tomography application was to estimate the void fraction, which is the proportion of gas and liquid in the image. With the proposed approach such goal variables can be estimated directly without explicit reconstruction of the image. The bottom row in Table 3 shows the relative absolute error in estimating the void fraction directly from the projections of the potential signals. Note that most of the eigen images in Fig. 3 have zero mean, so that they only code the shape of the distribution and make no contribution to the void fraction of the reconstruction. Hence the void fraction is clearly a lower dimensional subproblem of the whole reconstruction problem. Consequently the void fraction can be estimated to higher
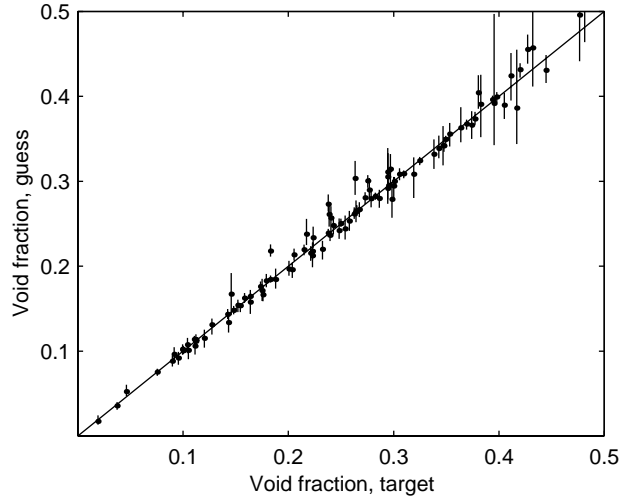

Figure 7: Scatterplot of the void fraction estimate with 10% and 90% quantiles.

accuracy directly from the measurements (see also [3]).

With Bayesian methods we can easily calculate confidence intervals for outputs. Fig. 7 shows the scatter plot of the void fraction versus the estimate by the Bayesian neural network. The 10% and 90% quantiles are computed directly from the posterior distribution of the model output.

5   Robustness to Noise

A special virtue of the solution proposed here is very high robustness to noise. Similar property of the neural network inverse was also reported in [7]. In the current approach the PCA projection of the potential signal and images contributes to the suppression of noise effects, as uncorrelated noise is also largely uncorrelated with the eigenvectors of the signals.
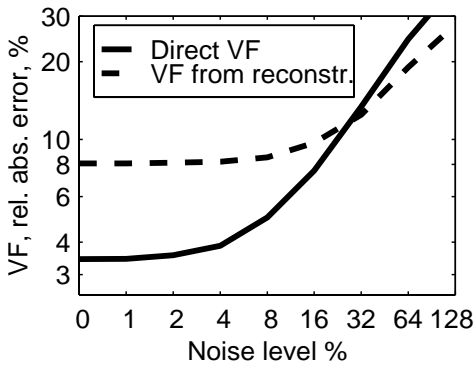
Figure 8: Effect of additive Gaussian noise to estimation of void fraction directly and from the reconstructed image.
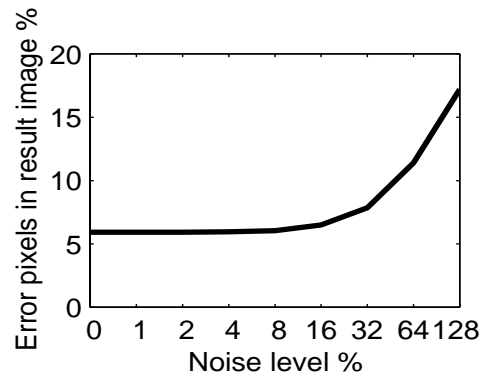

Figure 9: Effect of additive Gaussian noise to the reconstruction of the images.

Fig. 8 shows the effect of the noise on the inputs to the direct estimation of the void fraction. The noise was additive Gaussian noise with standard deviation given as percentage of the maximum amplitude of the potential signal. Fig. 9 shows the effect of noise to the image reconstruction results. Note that the expected noise level in industrial environment is about 2–5 %, which should have no significant effect to the inverse solutions by the proposed techniques.

6 Conclusion

In this contribution we have presented a method for solving the ill-posed inverse problem in electric impedance tomography with Bayesian neural networks.

With the proposed system

- the inverse can be computed in a feedforward manner, facilitating real-time monitoring of the process

- the image resolution can be chosen independently of the inverse model

- prior knowledge can be used to build the autocovariance model

- the solution is demonstrated to be highly immune to noise

- estimation of some target variables, such as the void fraction, may be applicable directly without the actual image reconstruction

- we can easily calculate confidence intervals for outputs

- correct model complexity is controlled by the Bayesian methods

Currently we are preparing tests for the method with real data in cooperation with the industrial partner of the project.

References

[1] Adler, A. & Guardo, R. (1994). A neural network image reconstruction technique for electrical impedance tomography. *IEEE Transactions on Medical Imaging*, 13(4):pp. 594–600.

[2] Bishop, C. M. (1995). *Neural Networks for Pattern Recognition*. Oxford University Press.

[3] Lampinen, J., Vehtari, A. & Leinonen, K. (1999). Using Bayesian neural network to solve the inverse problem in electrical impedance tomography. In *Proceedings of 11th Scandinavian Conference on Image Analysis SCIA'99*. Kangerlussuaq, Greenland.

[4] Neal, R. M. (1996). *Bayesian Learning for Neural Networks*, vol. 118 of *Lecture Notes in Statistics*. Springer-Verlag.

[5] Neal, R. M. (1998). Assessing relevance determination methods using DELVE. In C. M. Bishop, ed., *Neural Networks and Machine Learning*, vol. 168 of *NATO ASI Series F: Computer and Systems Sciences*. Springer-Verlag.

[6] Ni, X., Simons, S. J. R., Williams, R. A. & Jia, X. (1997). Use of PCA and neural network to extract information from tomographic images for process control. In *Proc. Frontiers in industrial process tomography*, vol. II, pp. 309–314. Engineering Foundation, New York, USA.

[7] Nooralahiyan, A. Y. & Hoyle, B. S. (1997). Three-component tomographic flow imaging using artificial neural network reconstruction. *Chemical Engineering Science*, 52(13):pp. 2139 – 2148. See also http://www.elec-eng.leeds.ac.uk/staff/een6njb/Research/processtom.html.

[8] Vauhkonen, M., Kaipio, J., Somersalo, E. & Karjalainen, P. (1997). Electrical impedance tomography with basis constraints. *Inverse Problems*, 13(2):pp. 523–530.